Available online at www.sciencedirect.com
ScienceDirect
Aquacultural Engineering 35 (2006) 218–227
aquacultural engineering
www.elsevier.com/locate/aqua-online

# Extracting fish size using dual underwater cameras

C. Costa [a,*], A. Loy [a], S. Cataudella [a], D. Davis [b], M. Scardi [a]

[a] *Aquaculture and Experimental Ecology Laboratory, Biology Department, University of Rome Tor Vergata, Via della Ricerca Scientifica, 00133 Rome, Italy*

[b] *Monterey Bay Aquarium Research Institute (MBARI), 7700 Sandholdt Road, Moss Landing, CA 95039-9644, USA*

Received 27 December 2004; accepted 9 February 2006

**Abstract**

The definition of a remote system in the monitoring of fin fish growth rate and shape change relies on the development of the appropriate optical ranging system and the automation of data collection. Among the available technologies, a dual camera optical ranging system is presented as the most suited for fish size remote estimation. Images are collected via a submergible low-priced dual camera module connected to a portable waterproof PC equipped with two frame grabbers. Two images are synchronically collected and, with the system parameters (focal length of both cameras, distance between the two cameras, vertical and horizontal tilt and relative rotation of the two cameras), are used to collect data of fish size and shape. A Neural Network is built to correct the error of measurement. A geometric algorithm is developed to filter fish images and elliptic Fourier analysis of automatically collected fish outline coordinates is proposed as a tool of shape analysis. For all other fish orientations, landmarks (homologous points) are collected on fish outlines and evident structures: landmark configurations relative to each fish are then rotated using the system parameters. The proposed system can be used in the monitoring of sea-based fish farming facilities, especially those which are permanently submerged, reducing mortality and stress due to fish sampling and limiting divers intervention. By its application in the study of wild population, the system can be useful in the characterization of fish communities and population dynamics, supporting traditional visual census techniques with a tool which allows for continuous, remote and automatic data collection.


*Keywords:* Aquaculture; Dual cameras; Sea cages; Neural network; 3D reconstruction; Fish size

## 1. Introduction

Accurate information on size and shape of wild and cultured fish populations is fundamental to the management of harvesting and is essential in aquaculture facilities to enable effective management of feeding regimes, grading times and ultimately the optimum time to harvest the stock (Beddow et al., 1996). Monitoring of length and age permit estimates of recruitment to fished populations, fishing intensity and rates of recovery from fishing or other disturbances.

In recent years there has been a trend towards aquaculture activities based on off-shore submerged sea cages. These facilities are not a convenient location for monitoring reared fish, and they can also become inaccessible because of rough sea and bad weather conditions. Actually, the most common way of estimating fish biomass is by directly sampling part of the reared fish stock or by visual census carried out by SCUBA divers. However, these methods may stress fish (Pickering and Christie, 1981; Maule et al., 1989) leading to scale as well as other related damages.Conventional still photography and video imagery have been widely adopted in the aquatic sciences for non-invasively

* Corresponding author. Tel.: +39 06 7259 5972; fax: +39 06 7259 5965.
*E-mail address:* corrado_costa@libero.it (C. Costa).

0144-8609/$ – see front matter © 2006 Elsevier B.V. All rights reserved.
doi:10.1016/j.aquaeng.2006.02.003

counting and measuring organisms underwater (Boland and Lewbell, 1986; Hamner et al., 1987, 1988; Vrana and Schwartz, 1989; Naiberg et al., 1993; Petrell et al., 1997). For instance, stereo-photography has been used in situ to measure recruitment, growth and mortality of coral colonies (Done, 1981), length of free-swimming sharks (Klimley and Brown, 1983) and dolphins (Brager and Chong, 1999). Recently, non-invasive techniques, included stereo-photography, have been developed for predicting salmon biomass remotely in the field (Naiberg et al., 1993; Beddow et al., 1996; Hockaday et al., 1997; Boucher and Petrell, 1999; Hockaday et al., 2000) and reef fish (Harvey et al., 2001a,b). These methods use calibration equations that link lateral measurements (truss and conventional) to mass estimates, and rely on the acquisition of suitable stereo-images of fish in tanks or cages (Martinez de Dios et al., 2003). Beddow et al. (1996) successfully used stereo-imaging techniques to remotely estimate salmon biomass to within 0.4% of the real value. Furthermore, there are some commercial devices for monitoring fish biomass in cages, such as Vaki's biomass counter, that use frames through which fish are forced to pass into.

Recent, rapid technological enhancements in video cameras improved the utility and accuracy of measurements by means of such systems (Davis and Pilskaln, 1992; Harvey and Shortis, 1996, 1998; Harvey et al., 2003), complementing the advantages of predictable precision of measurements, opportunity for motion sequence capture, and archival storage of digital images (Ruff et al., 1995; Van Rooij and Videler, 1996; Petrell et al., 1997; Pippy et al., 1997). These video techniques can be readily adapted for use by SCUBA divers (Harvey et al., 2001a,b) or mounted on remotely operated vehicles and submersible platforms (Baldwin and Newton, 1982; Li et al., 1996; Pitcher et al., 1999) to capture images at depths beyond those accessible by SCUBA divers.

In this study a dual camera system is proposed to automatically extract information on shape and size of fish. An image analysis algorithm was developed to preprocess images, i.e. to filter out images in which no fish were found and to extract fish outlines from others. A vector algorithm was then used to reconstruct the 3-dimensional coordinates of relevant landmarks on the basis of the 2D coordinates in a pair of stereo images.

Although in theory this approach may provide an exact reconstruction of the geometrical properties of the objects depicted in the images, it is influenced by several sources of error in real world applications. For instance, optical properties of camera lenses may be slightly biased, thus causing some distortion in the outer part of the images. Therefore, an empirical algorithm, based on an Artificial Neural Network, was used to correct the coordinates obtained from the vector algorithm, thus reducing the measurement error.

## 2. Materials and methods

### 2.1. Hardware

Image recording for the dual video analysis was performed by two b/w Urmet Sideltronix EX 1090/105 analogic video cameras (optical resolution: 752 × 582 pixel; sensitivity to light: 0.08 lx; s/n ratio >48 dB) in stainless steel waterproof housings. The two cameras were connected, synchronized and powered via cable with two Frame Grabbers DT3155 in a waterproof transportable computer. The maximum frequency of acquisition for coupled synchronous frames was 2 per second.

The cameras were mounted on a bar. The right camera was fixed on a goniometer to measure the horizontal tilt angle. The distance between cameras could also be changed. Focal length of the cameras was 8.0 mm. This configuration gave a 0.59 m × 0.47 m overlapping area in the field of view in water at a 0.6 m distance. The selected relative camera angle chosen was a trade off between field of view and measurement precision. A more acute convergence would decrease the useable field of view, but improve the measurement precision (Harvey and Shortis, 1996).

### 2.2. Software

The general software procedure is described in Fig. 1. Synchronous pairs of frames (left and right) were grabbed and stored. At first only left frames were automatically analyzed to determine whether they were likely to contain any images of fish suitable for further analysis or not.

Both left and right images that contained potential targets were then filtered using a procedure aimed at extracting the fish outlines. Each fish has different geometry depending on the species and, among specimens belonging to the same species, depending on aspect and individual shape. The geometrical properties (namely, area, major axis length and circularity) of each fish were then extracted. Underwater images were acquired at 11:00 a.m. at 10 m depth, while water turbidity was rather low (Disco Secchi >10 m). The first step in the filtering procedure involved two filters: Trimmed Mean 5 × 5 and Sobel. Trimmed Mean 5 × 5 excludes the three smallest and three largest values in each 5 × 5 neighborhood and averages the remaining ones reducing the high frequencies of noise without

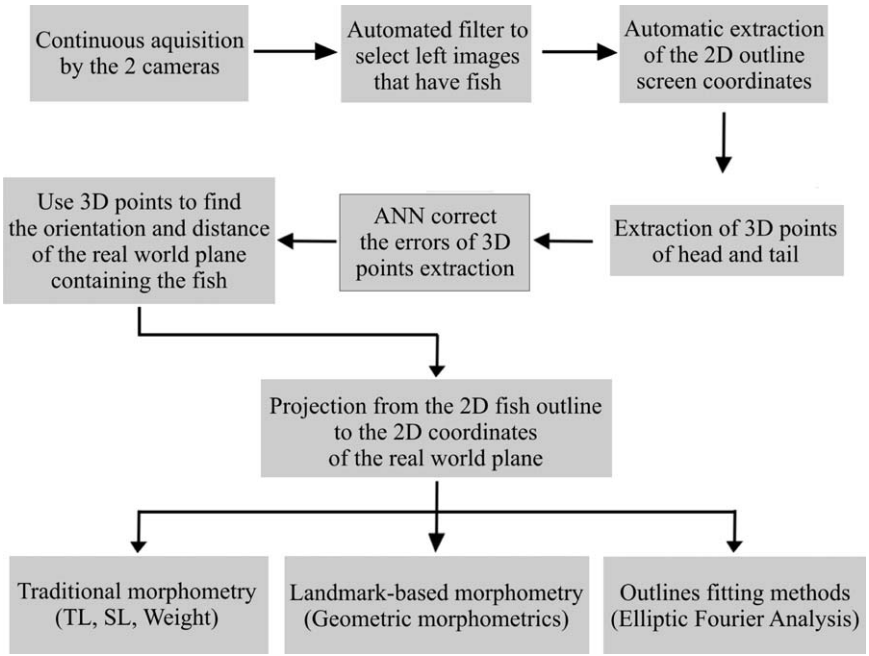


Fig. 1. General software procedure.

degrading edges or smoothing gradients intensity. Sobel filter detects edges replacing the center pixel of a $3 \times 3$ neighborhood with the square root of the sum of squares of the vertical and horizontal gradients. After applying these filters, the images were binarized using a 24 value in the 8 bits gray-scale image as the threshold. This value was empirically defined, and it was applied to all the images processed.

In order to enhance the outlines, making them less fragmented, each image was then processed by means of a set of morphological filters, namely Erode (foreground pixels that are connected on any side or any corner to a background pixel are eliminated), Dilate (is the opposite of erosion: after segmenting a gray scale image into a binary image, the dilate operation identifies background pixels that are 8-connected to a foreground pixel and changes them to foreground), Close (a dilation followed by an erosion), and Fill (fills holes in foreground regions).

To discriminate fish-like objects in each image three geometrical properties were used: area, major axis length and circularity (these properties are species-specific and may be used to support species identification procedures). Objects whose outlines did not fit into appropriate ranges of these geometrical properties were not considered, while outline coordinates were extracted only from objects that matched the "fish" criteria.

In case there were no complete fish inside the left image the filtering procedure automatically erased both left and right images.

On the contrary, in both images containing fish-like outlines, location and orientation, in 3-dimensional real world coordinates, of candidate fish targets was defined by selecting several corresponding points in both images and then applying a geometrical algorithm. Model based analysis software then attempts to identify the boundary of the fish and locate it in 3D space. If a satisfactory fit is achieved, key measurement points on this boundary are identified and the distances between them calculated.

In order to explain the rationale supporting the geometrical algorithm that returned estimates of point positioning based on a pair of images, let us assume that all vectors are represented in some convenient 3-dimensional coordinate system. However, being vector based, the derivation below is independent of the chosen orthogonal coordinate system. In practice, it will be useful to have local coordinate systems for each camera, and compute the vectors below from these local coordinates.

Assuming that the relative positions and orientations of the cameras are known, as well as the focal lengths or equivalently the angle width of view of each camera, we as well as define (Fig. 2):

$\vec{u}_1$ a unit vector along the direction of the axis of camera #1
$\vec{u}_2$ a unit vector along the direction of the axis of camera #2
$d_1$ the scalar focal length of camera #1measured in the direction-$\vec{u}_1$
$d_2$ the scalar focal length of camera #2 measured in the direction-$\vec{u}_2$
$\vec{w}_1$a 3-D vector from the screen origin of the camera screen to the image point of the target in camera #1

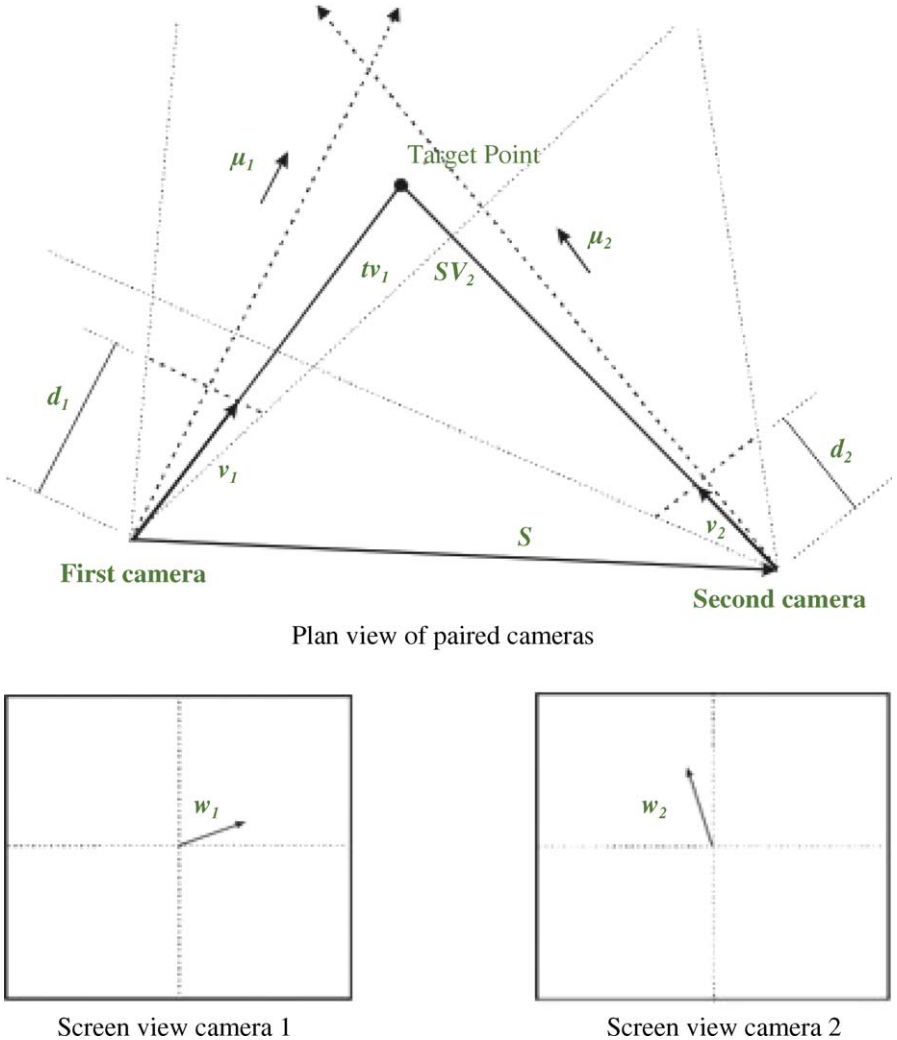


Fig. 2. Plan view of paired cameras and screen of image cell view.

$\vec{w}_2$ a 3-D vector from the origin of the right camera screen to the image point of the target in camera #2

$\vec{S}$ a 3-D vector from the origin of camera #1 screen to the origin of camera #2 screen

Since $\vec{u}_i$ and $\vec{w}_i$ $(i = 1, 2)$ are orthogonal:

$$\vec{\boldsymbol{u}}_1 \cdot \vec{\boldsymbol{w}}_1 = 0 \qquad \boldsymbol{u}_2 \cdot \boldsymbol{w}_2 = 0 \tag{1}$$

Since both cameras can image the target point, we can write a vector equation expressing this fact in terms of the camera orientations, distance between the cameras, camera focal lengths $d_1$ and $d_2$, and the vectors that describe the screen position of the imaged target point in each camera. By the definitions of the above vectors it follows that vectors pointing in the direction of the target point from the left and right cameras, respectively, are:

$$\vec{\boldsymbol{v}}_1 = (\vec{\boldsymbol{w}}_1 + d_1 \vec{\boldsymbol{u}}_1) \text{ and } \vec{\boldsymbol{v}}_2 = (\vec{\boldsymbol{w}}_2 + d_2 \vec{\boldsymbol{u}}_2) \tag{2}$$

It then follows that there must exist *positive* scalars $s$ and $t$ such that:

$$t\vec{\boldsymbol{v}}_1 = \vec{\boldsymbol{S}} + s\vec{\boldsymbol{v}}_2 \tag{3}$$

or,

$$t\vec{\boldsymbol{v}}_1 - s\vec{\boldsymbol{v}}_2 = \vec{\boldsymbol{S}} \tag{4}$$

We also have some further constraints on the above vectors that express the assumption that the target point

is in *front* of both cameras.

$$t\vec{v}_1 \cdot \vec{u}_1 > d_1 \text{ and } s\vec{v}_2 \cdot \vec{u}_2 > d_2 \tag{5}$$

We can derive scalar equations in the two unknowns $s$, $t$ if we take the dot product of vector Eq. (4) with the vectors $\vec{v}_1$ and $\vec{v}_2$.

Thus,

$$\begin{bmatrix} \vec{v}_1 \cdot \vec{v}_1 & -\vec{v}_2 \cdot \vec{v}_1 \\ \vec{v}_1 \cdot \vec{v}_2 & -\vec{v}_2 \cdot \vec{v}_2 \end{bmatrix} \cdot \begin{pmatrix} t \\ s \end{pmatrix} = \begin{pmatrix} \vec{S} \cdot \vec{v}_1 \\ \vec{S} \cdot \vec{v}_2 \end{pmatrix} \tag{6}$$

This has a unique solution if and only if the vectors $\boldsymbol{v}_1$ and $\boldsymbol{v}_2$ are *not parallel*. The scalars $t$ and $s$ can be easily calculated by Cramer's Rule, and either may be used in the vector equations

$$\vec{P}_1 = t(\vec{w}_1 + \mathrm{d}\vec{u}_1) \text{ and } \vec{P}_2 = s(\vec{w}_2 + \mathrm{d}\vec{u}_2) \tag{7}$$

to obtain an expression for the 3D coordinates of the target point $\vec{P}_1$ (or $\vec{P}_2$) relative to the origin of the left (or right) camera's nodal point, respectively.

Cramer's rule states that:

$$t = \frac{\begin{vmatrix} \vec{S} \cdot \vec{v}_1 & -\vec{v}_2 \cdot \vec{v}_1 \\ \vec{S} \cdot \vec{v}_2 & -\vec{v}_2 \cdot \vec{v}_2 \end{vmatrix}}{\begin{vmatrix} \vec{v}_1 \cdot \vec{v}_1 & -\vec{v}_2 \cdot \vec{v}_1 \\ \vec{v}_1 \cdot \vec{v}_2 & -\vec{v}_2 \cdot \vec{v}_2 \end{vmatrix}} \tag{8}$$

and

$$s = \frac{\begin{vmatrix} \vec{v}_1 \cdot \vec{v}_1 & S \cdot \vec{v}_1 \\ \vec{v}_1 \cdot \vec{v}_2 & S \cdot \vec{v}_2 \end{vmatrix}}{\begin{vmatrix} \vec{v}_1 \cdot \vec{v}_1 & -\vec{v}_2 \cdot \vec{v}_1 \\ \vec{v}_1 \cdot \vec{v}_2 & -\vec{v}_2 \cdot \vec{v}_2 \end{vmatrix}} \tag{9}$$

This geometric algorithm is used within the Point Locator tool, an Optimas™ program developed at MBARI that computes the *XYZ* point from the images representing the two cameras views.

Although the geometric algorithm is based on a sound rationale, it might fail in practical applications, e.g. because of optical aberrations due to lens characteristics (see, for instance, Fig. 3). Therefore, developing an adequate algorithm for correcting the 3D positioning data obtained from the dual camera system was a critical prerequisite for practical applications. A heuristic approach was developed to tackle this problem, using Artificial Neural Networks (ANNs).

ANNs are very effective in many applications, and are particularly useful as generalized non-linear regression tools. The term artificial neural network derives from the analogy of its structure with that of a biological neural network – weighted links being analogous with axons and the processing units being analogous with neurons (Robertson and Morison, 1999). ANNs can be effective at solving problems where no clear-cut solutions exists (e.g. no theoretical models), can be exceptionally robust against noise, and are immune to violations of assumptions that invalidate many traditional analytical method (Masters, 1994).

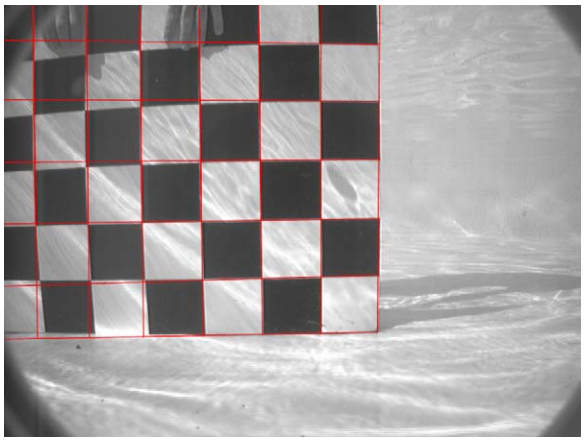

Fig. 3. Image of a grid with optical aberrations due to lens characteristics. In red the right grid configuration.

In this study, the ANNs were used to post-process data from the geometric algorithm. Given positioning data ($X$; $Y$; $Z$ coordinates) from a set of objects whose location in the 3D space was known, distance between cameras and focal length of the lenses, the ANNs were trained to return corrected positioning data. A total number of 319 couple of images with several measured objects were used to extract data for the ANNs training, validation and testing.

The most common combination of ANN architecture and training algorithm was used, i.e. multilayer perceptrons and error back-propagation algorithm. The best architecture of the ANNs was empirically defined after a set of test runs in which different numbers of hidden layer nodes were used. The final ANNs, one for each focal length, had a 4-15-3 architecture, i.e. 4 input nodes (measured $x$, $y$, $z$ and distance between cameras), 15 nodes in the hidden layer and 3 output nodes (corrected $x$, $y$ and $z$). Strategies for avoiding overtraining, which is likely to happen in ANNs with many hidden nodes, were also adopted: namely the addition of white noise to the network inputs and the early stopping of the training phase based on the minimization of the mean square error (MSE) relative to an independent validation data set. The training of each ANN was carried out during two subsequent phases: in the first one the ANNs were trained using a fast learning strategy (learning rate = 0.9 and momentum = 0.1), whereas during the second phase they were fine-tuned

(learning rate = 0.1, momentum = 0.9). In both cases the training procedure was repeated 1000 times and the best performing ANN was selected based on an independent test set. For each focal length the training set included 200 patterns, while 100 patterns were used as a validation set to avoid overtraining and 200 more patterns were used as a test set, i.e. for evaluating the ANN performance after the training phase.

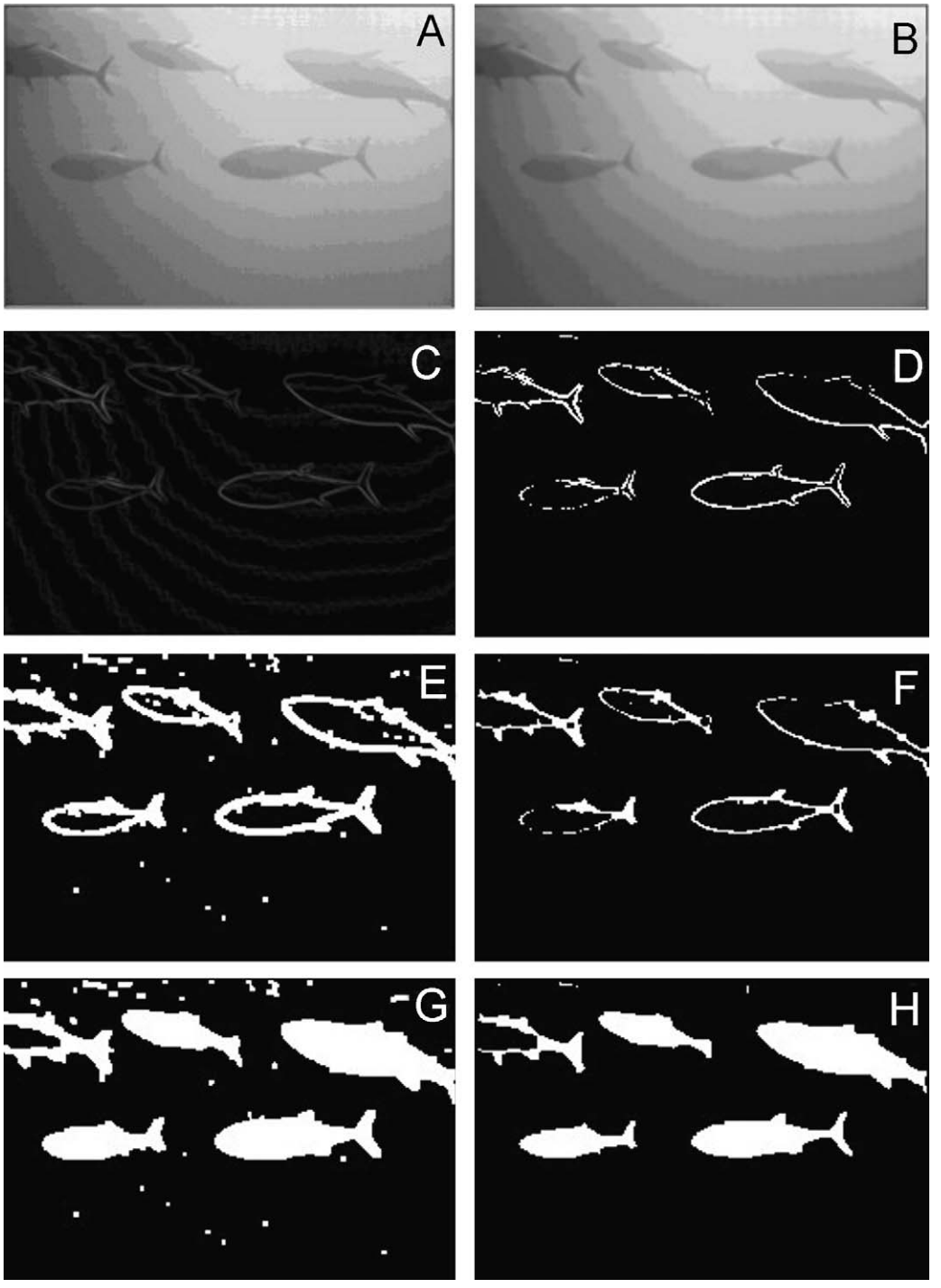


Fig. 4. Sequence of filtering: (A) original image; (B) image after Trimmed Mean 5 × 5 filter; (C) image after Sobel filter; (D) image after threshold; (E) image after three ''close''; (F) image after three ''dilate''; (G) image after other three ''close'' and three ''fill''; (H) final image after three erode.

## 3. Results

### 3.1. Image pre-processing

The results of the image filtering procedure are shown in Fig. 4, using a sample image from a series acquired in a floating cage located in Southern Italy (Favignana, Sicily) in November 2000, where northern bluefin tunas (*Thunnus thynnus thynnus*; Linnaeus, 1758) were reared.

The sample image (Fig. 4A) showed in this section was extracted from a set of over 300 images of a stock of Northern Bluefin Tuna (*Thunnus thynnus thynnus*; Linnaeus, 1758).

The first passage of filtering applied two filters: Trimmed Mean 5 × 5 (Fig. 4B) and Sobel (Fig. 4C). After applying these filters, the image was binarized using a threshold (Fig. 4D). The resulting image was then processed using a sequence of morphological filters. In fact three Close filtering steps (Fig. 4E), followed by three Dilate steps (Fig. 4F) were applied. Then, three more Close, three Fill (Fig. 4G) and three Erode (Fig. 4H) were performed sequentially.

The final result of the above image processing procedure is shown in Fig. 5, in which both the original image and the outlined objects are shown as extracted by the filters. To discriminate fish-like objects in each image geometrical properties of the outlines were then considered.

### 3.2. Image processing

Relevant landmarks in the fish outlines were then converted into point coordinates by the geometric Point Locator algorithm. Coordinates estimated by means of the geometric algorithm were compared with the observed (i.e. known) coordinates as shown in Fig. 6. It is possible to observe a good agreement between observed and estimated values for all $x$, $y$ and $z$ coordinates. Errors relative to the $y$-axis (Fig. 6B) were slightly larger than errors on other axes. Moreover, errors

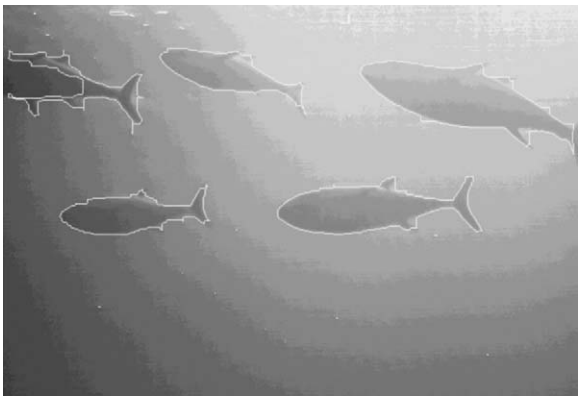

Fig. 5. Final result of the image processing: the original image is overlapped to the outlined object extracted by the filters.

in $x$ coordinates tended to increase according to distances from the center of the image, while $y$ coordinates tended to be systematically underestimated by the geometric algorithm. The mean square errors of the coordinates obtained from the geometric algorithm were 189.9, 82.2 and 121.1 for $x$, $y$ and $z$ axes, respectively.

### 3.3. ANNs correction

ANNs provided very good results in correcting the positioning data, as shown in Fig. 7A–C. The accuracy of the corrections was very good, as shown by the limited scattering of the points around the unit slope line, which indicates an almost perfect fit. The mean square errors of the ANN-corrected positioning data were 6.1, 2.0 and 54.8, respectively, for $x$, $y$ and $z$ axes.

However, the accuracy of the correction was not independent of the true positioning of the objects, as the efficiency of the image acquisition varied with respect to distance from the cameras, distance from the cameras' midline and aspect of the targets. The relative error in the estimated size of a target, that is the most practical measure for accuracy of the system, also varied, but it was obviously related to the absolute size of the target. In Fig. 8 the relative error in length

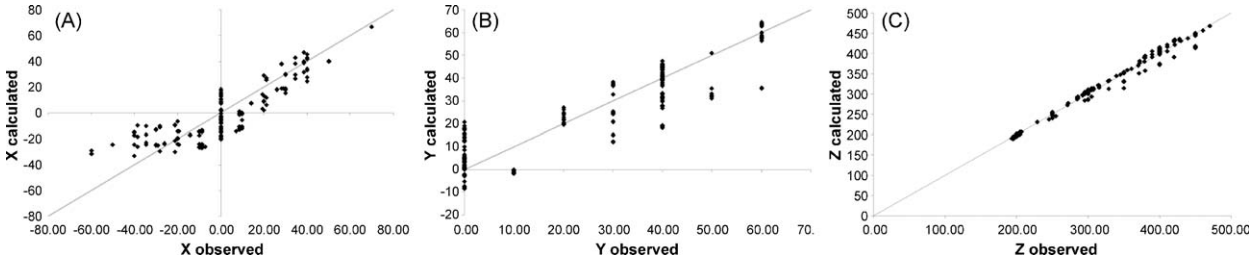


Fig. 6. Comparison between observed (i.e. true) and calculated with the geometric algorithm $x$ (A), $y$ (B) and $z$ (C) coordinates.

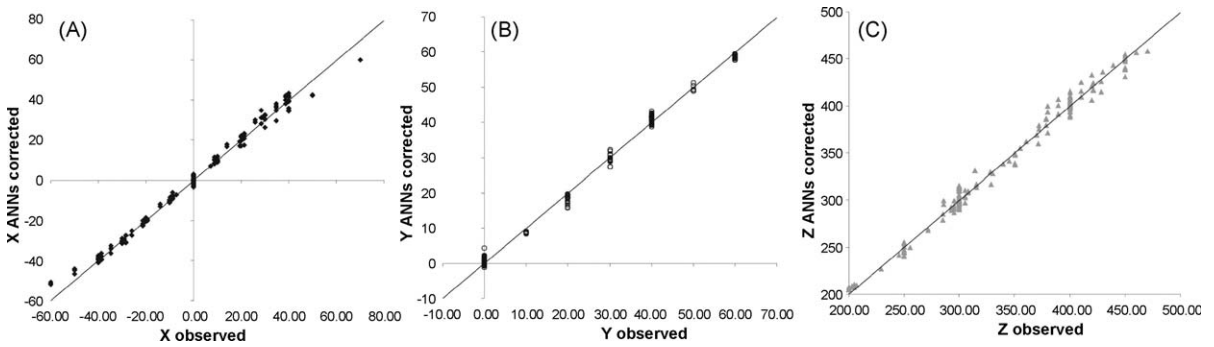


Fig. 7. Comparison between observed (i.e. true) and ANNs corrected $x$ (A), $y$ (B) and $z$ (C) coordinates.

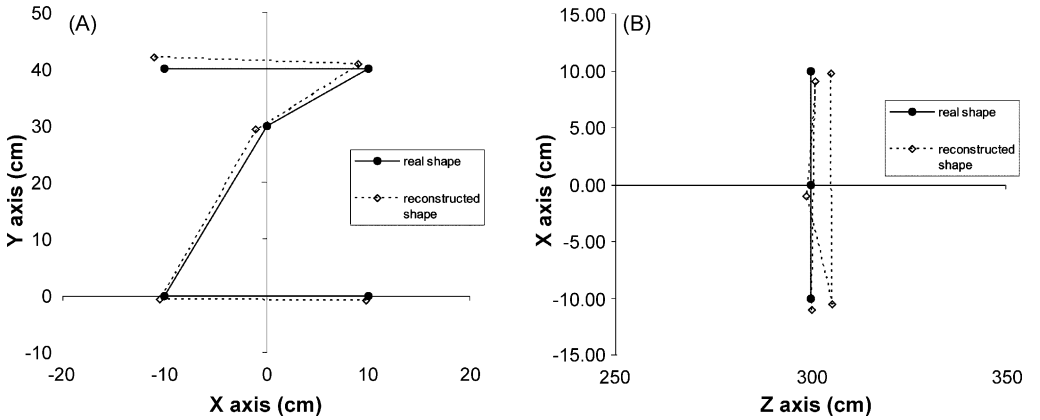


Fig. 8. A reconstructed shape compares to its real counterpart after the correction.

estimates is shown. Test targets were different in length and all targets had the same y coordinate at both ends, while only $x$ and $z$ coordinates varied. It is clear that smaller targets were more difficult to measure and that the relative error was larger.

In order to highlight differences in size and shape extraction based on the geometrical algorithm only and on the ANN-corrected procedure, the image of a tuna model of 180 cm of fork length (FL) was analyzed. The true tuna model shape is shown in Fig. 9A, while in Fig. 9B the landmarks obtained from the geometrical algorithm are shown. The original tuna image was then morphed on the basis of these landmarks to show the way the geometrical algorithm distorted the fish shape. The error in the length estimate was about 5% of the fish true length. In Fig. 9C the same fish image was post-processed by the ANN correction. It is very clear that the overall shape of the fish is much closer to the original one, while the error in the length estimates is almost negligible.

A simpler comparison between a true object and its reconstructed counterpart is shown in Fig. 8. A Z-shaped object was used, whose measures were obviously known, and the ANN-based correction was performed on the estimates of its coordinates as obtained from the geometric algorithm. The two sub-plots show the projection of the Z-shaped object on the

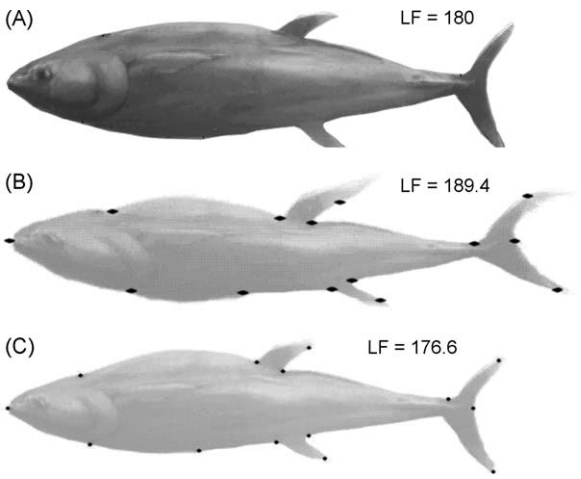


Fig. 9. (A) Size (FL) and shape of a tuna model; (B) an example of size and shape extracted from a couple of images with the geometric algorithm; (C) the correspondent size and shape corrected with ANNs.

xy and xz planes, respectively. The reconstructed shape is very similar to the real one, and the distances between homologous points are small, ranging from 1.6 (point on the midline) to 5.6 cm (lower left point) (Fig. 9).

## 4. Discussion

This study showed that a dual camera system can be used to make accurate, non-invasive in situ measurement of fish. The overall accuracy of the measurements, especially after the ANN correction, is more than adequate for practical applications.

Three-dimensional information can be extracted from fish images and the resulting outlines, linear measures or landmarks, corrected with ANNs, can be analyzed by means of conventional shape analysis techniques, such as geometric morphometric analysis or elliptic Fourier analysis (Loy et al., 2000).

There are obvious benefits for fisheries, aquaculture and farm managers in the use of an underwater video measurement system without disturbances related to capture and handling. Moreover, the growth of aquaculture activities in off-shore cages highlights the need for monitoring devices and procedures that can be remotely operated or that can acquire relevant information while unattended. The commercial devices for monitoring fish cage biomass that use frames in which fish are forced to pass into present evident disadvantages with respect to methods based on image analysis, and many studies, like this one, pointed out new strategies for tackling those problems (Harvey et al., 2003).

A different version of the Point Locator algorithm has also been used with a single moving camera to get the size of marine organisms in mid water transects by an ROV (Davis and Edgington, 2004). In this application it was assumed that the target did not move in the time interval between the two shots taken by a single moving camera.

Regarding rapid development of techniques in 3D image estimation system on one side and increase in necessity of quantitative measurement in animal population on the other side, this type of in situ online automatic monitoring system has drawn a strong attention from specialists involved in ecosystem management, and the results from this study would contribute to broadening the scope of automatic quantification method in ecological and behavioural monitoring.

## Acknowledgments

This study was supported by a grant from the Ministero Italiano per le Politiche Agricole e Forestali (Law 41/82). Authors would like to acknowledge Dott Maurizio Giganti and Dott Davide Cascione that help in the diving operations.

## References

Baldwin, R.A., Newton, I., 1982. A proposed system for underwater photogrammetry from a manned submersible. Int. Arch. Photogramm. 24 (5), 39–52.

Beddow, T.A., Ross, L.G., Marchant, J.A., 1996. Predicting salmon biomass remotely using a digital stereo-imaging technique. Aquaculture 146 (3–4), 189–203.

Boland, G.S., Lewbell, G.S. (1986). The estimation of demersal fish densities in Biological surveys using underwater television systems. In: Oceans '86, IEEE Publishing Services, New York, 1. Systems, Structures and Analysis, 9–13.

Boucher, E., Petrell, R.J., 1999. Swimming speed and morphological features of mixed populations of early maturing and non-maturing fish. Aquacult. Eng. 20, 21–35.

Brager, S., Chong, A.K., 1999. An application of close range photogrammetry in dolphin studies. Photogramm. Record 17 (93), 503–517.

Davis, D.L., Edgington, D.R., 2004. Getting size scale from a single moving underwater camera. In: ASLO-TOS Ocean Research Conference, Honolulu, Hawaii, February 2004, pp. 15–20.

Davis, D., Pilskaln, C., 1992. Measurements with underwater video: camera field width calibration and structured lighting. J. Mar. Technol. Soc. 26 (4), 13–19.

Done, T.J., 1981. Photogrammetry in coral reef ecology: a technique for the study of change in coral reef communities, 2. In: Proceedings of the Fourth International Coral Reef Symposium, Manila, pp. 315–320.

Hamner, W., Kristof, E., Chandler, A. (1987). 3-D video and computer analysis of fish schooling. In: Oceans '87 Proceedings: the ocean-an international work place. September 28–October 1, IEEE Service Centre, 1232–1233.

Hamner, W., Lipton, L., Kristof, E., Leonhardi, P. (1988). Three dimensional video as an underwater tool. In: D., Holloway (Ed.), Underwater imaging. Proceedings of the International Society for Optical Engineering, 18 August, San Diego, California. SPIE, 980 Underwater Imaging, 2–9.

Harvey, E., Cappo, M., Shortis, M., Robson, S., Buchanan, J., Speare, P., 2003. The accuracy and precision of underwater measurement of length and maximum body depth of southern bluefin tuna (*Thunnus maccoyii*) with a stereo-video camera system. Fish. Res. 63, 315–326.

Harvey, E.S., Fletcher, D., Shortis, M.R., 2001a. A comparison of the precision and accuracy of estimates of reef-fish length made by divers and a stereo-video system. Fish. Bull. 99 (1), 63–71.

Harvey, E.S., Fletcher, D., Shortis, M.R., 2001b. Improving the statistical power of visual length estimates of reef fish: a comparison of divers and stereo-video. Fish. Bull. 99 (1), 72–80.

Harvey, E.S., Shortis, M.R., 1996. A system for stereo-video measurement of subtidal organisms. J. Mar. Technol. Soc. 29 (4), 10–22.

Harvey, E.S., Shortis, M.R., 1998. Calibration stability of and underwater stereo-video system: Implications for measurement accuracy and precision. J. Mar. Technol. Soc. 32 (2), 3–17.

Hockaday, S., Ross, L.G., Tillett, R., 1997. Using stereo image pairs to measure mass in strains of Atlantic salmon, *Salmo salar* L. In:

Augousti, A.T., White, N.M. (Eds.), Sensors and their Applications VIII. Bristol Institute of Physics, pp. 21–26.

Hockaday, S., Beddow, T.A., Stone, M., Hancock, P., Ross, L.G., 2000. Using truss networks to estimate the biomass of *Oreochromis niloticus*, and to investigate shape characteristics. J. Fish Biol. 57, 981–1000.

Klimley, A.P., Brown, S.T., 1983. Stereophotography for the field biologist: measurement of lengths and three-dimensional positions of free swimming sharks. Mar. Biol. 74, 175–185.

Li, R., Li, H., Zou, W., Smith, R.G., Curran, T.A., 1996. An underwater digital photoegrammetric system for fishery goematics. Int. Arch. Photogramm. Remote Sens. 31 (B5), 524–529.

Loy, A., Busilacchi, S., Costa, C., Ferlin, L., Cataudella, S., 2000. Comparing geometric morphometric and outline fitting methods to monitor fish shape shape variability of *Diplodus puntazzo* (Teleostea: Sparidae). Aquacult. Eng. 21 (4), 271–283.

Martinez de Dios, J.L., Serna, C., Ellero, A., 2003. Computer vision and robotics techniques in fish farms. Robotica 21, 233–243.

Masters, T., 1994. Signal and Image Processing with Neural Networks. John Wiley, New York.

Maule, A.G., Tripp, R.A., Kaatari, S.L., Schreck, C.B., 1989. Stress alters immune function and disease resistance in chinook salmon *Oncorhynchus tshawytscha*. J. Endocrinol. 120, 135–142.

Naiberg, A., Petrell, R.J., Savage, C.R., Neufeld, T., 1993. Noninvasive fish size assessment method for tanks and sea cages using stereo-video. In: Wang, J.K. (Ed.), Techniques for Modern Aquaculture. American Society of Agricultural Engineers, St. Joseph, M.I., pp. 372–381.

Petrell, R.J., Shi, X., Ward, R.K., Naiberg, A., Savage, C.R., 1997. Determining fish size an swimming speed in cages and tanks using simple video techniques. Aquacult. Eng. 16, 63–84.

Pickering, A.D., Christie, P., 1981. Changes in the concentration of plasma cortisol and thyroxine during sexual maturation of the hatchery reared brown trout *Salmo trutta* L. Gen. Comp. Endocrinol. 44, 487–496.

Pippy, J.H.C., Whelan, W.G., O' Connell, M.F., 1997. A field guide to counting and measuring salmonids using the Silhouette Imaging and Counting System (SIACS). Can. Manuscr. Rep. Fish. Aquat. Sci. 2386, 99.

Pitcher, C.R., Wassenberg, T.J., Smith, G.P., Cappo, M., Hooper, J.N.A., Doherty, P.J., 1999. Innovative new methods for measuring the natural dynamics of some structurally dominant tropical sponges and other sessile fauna. Memoirs of the Queensland Museum 44, 479–484.

Robertson, S.G., Morison, A.K., 1999. A trial of artificial neural networks for automatically estimating the age of fish. Mar. Freshwater Res. 50, 73–82.

Ruff, B.P., Marchant, J.A., Frost, A.R., 1995. Fish sizing and monitoring using a stereo image analysis system applied to fish farming. Aquacult. Eng. 14, 155–173.

Van Rooij, J.M., Videler, J.J., 1996. A simple field method for stereophotographic length measurement of free-swimming fish: merits and constraints. J. Exp. Mar. Biol. Ecol. 195, 237–249.

Vrana, K.J., Schwartz, J., 1989. Instrumented sled, ROV join to provide enhanced images of Edmund Fitzgerald. Sea Technol. 30 (12), 17–21.